PERMAFROST AND PERIGLACIAL PROCESSES
Permafrost and Periglac. Process. **28**: 391–404 (2017)
Published online 9 January 2017 in Wiley Online Library
(wileyonlinelibrary.com) DOI: 10.1002/ppp.1939

The Application and Evaluation of Simple Permafrost Distribution Models on the Qinghai–Tibet Plateau

Shu-Ping Zhao,[1,2] *Zhuo-Tong Nan,*[1,3]* *Ying-Bing Huang*[4] *and Lin Zhao*[5]

[1] Key Laboratory of Virtual Geographic Environment of Ministry of Education, Nanjing Normal University, Nanjing, China
[2] State Key Laboratory of Frozen Soil Engineering, Cold and Arid Regions Environmental and Engineering Research Institute, CAS, Lanzhou, China
[3] Jiangsu Center for Collaborative Innovation in Geographical Information Resource Development and Application, Nanjing, China
[4] Research Center of Dongguan Geography Information and Planning, Dongguan, China
[5] Cold and Arid Regions Environmental and Engineering Research Institute, CAS, Lanzhou, China

ABSTRACT

The performance of simple permafrost distribution models widely used on the Qinghai–Tibet Plateau (QTP) has not been fully evaluated. In this study, two empirical models (the elevation model and mean annual ground temperature model) and three semi-physical models (the surface frost number model, the temperature at the top of permafrost model and the Kudryavtsev model) were investigated. The simulation results from the models were compared to each other and validated against existing permafrost maps of the entire QTP and in three representative areas investigated in the field. The models generally overestimated permafrost distribution in the investigated areas, but they captured the broad characteristics of permafrost distribution on the entire QTP, and performed best in areas with colder, continuous permafrost. Large variations in performance occurred at elevations of 3800–4500 m asl and in areas with thermally unstable permafrost. The two empirical models performed best in areas where permafrost is strongly controlled by elevation, such as eastern QTP. In contrast, the three semi-physical models were better in southern island permafrost areas with relatively flat terrain, where local factors considerably impact the distribution of permafrost. Model performance could be enhanced by explicitly considering the effects of elevation zones and regional conditions. Copyright © 2017 John Wiley & Sons, Ltd.

KEY WORDS: permafrost distribution; permafrost mapping; Qinghai–Tibet Plateau (QTP); model evaluation

INTRODUCTION

The simulation and prediction of permafrost distribution on the Qinghai–Tibet Plateau (QTP) is essential for supporting climatic studies and decision-making during the planning and design phases of engineering projects. A complete understanding of permafrost distribution there, however, remains unclear due to the limited number and high costs of field observations. Thus, permafrost models potentially provide an effective solution to map permafrost distribution in the region.

Several empirical and semi-physical models have been applied to map permafrost on the QTP. For example, Cheng developed an 'elevation model' to estimate the lower limit of permafrost in mountainous regions, by which Li and Cheng (1999) simulated the distribution of permafrost on the QTP. Nan *et al.*(2002) related mean annual ground temperature with elevation and latitude, and modelled the entire QTP using a regression approach. Wu *et al.* (2002) applied the temperature at the top of permafrost (TTOP) model to the QTP (Riseborough, 2002). Nan *et al.* (2013) modelled permafrost distribution on the western QTP using an enhanced surface frost number model. Ran *et al.* (2012) reviewed the permafrost distribution maps in China and attempted to develop an improved map by integrating them, although this was not convincing because the maps used were old and thus did not represent present-day conditions. Other mathematical methods such as the multivariate adaptive regression spline (MARS) method (Zhang *et al.,* 2013) and probabilistic method (Li *et al.,* 2009) have also been used for mapping permafrost distribution, and have been reported to perform well in small areas. Recently, land surface

* Correspondence to: Z.-T. Nan, Key Laboratory of Virtual Geographic Environment of Ministry of Education, Nanjing Normal University, Nanjing 210023, China. E-mail: nanzt@njnu.edu.cn

Received 4 February 2016
Revised 8 November 2016
Accepted 1 December 2016

models (LSMs) have been applied to simulate the thermal and hydrological state of frozen ground on the QTP at site scale (van der Velde *et al.,* 2009; Yang *et al.*, 2009; Xiao *et al.,* 2013) or in small regions (Chen *et al.,* 2015). Nevertheless, the lack of fine-resolution meteorological forcing data and detailed soil parameters severely challenges region-wide use of LSMs, which require many more data and parameters than empirical and semi-physical models. Therefore, simple models such as those examined in this study are still widely used, although their applicability has not yet been studied systematically.

We applied five simple models to map permafrost distribution on the QTP based on their academic recognition and practical use. Two are empirical models (an elevation model (ELEV) and a mean annual ground temperature model (MAGT)) and three are semi-physical (a surface frost number model (FROSTNUM), a temperature at the top of permafrost model (TTOP) and the Kudryavtsev model (K-MODEL)). The ELEV model and its variants are some of the most favoured models for mapping local permafrost distribution on the QTP (e.g. Li & Cheng, 1999; Cheng *et al.,* 2012). The MAGT model is the basis for the QTP region in the *Map of the Glaciers, Frozen Ground and Deserts in China* (1: 4000 000) (CAREERI/CAS, 2005), which is still referred to as a benchmark (e.g. Wang, 2009). The three semi-physical models have been used in recent publications (Juliussen & Humlum, 2007; Nan *et al.*. 2012; Luo *et al.,*2014). The K-MODEL forms the core of the GIPL 1.0 model (Riseborough *et al.,* 2008). The other empirical models such as MARS or the probability approach are not discussed as they are not generally applied to the entire QTP. We examined the performance of the five models by means of inter-comparison and validation against existing maps.

METHODS

Models

The ELEV model (Eqn 1) follows an exponential law to define the lower limit of permafrost occurrence H (m asl) with latitude φ (°) at high elevations using data from 1955 to 1984 in the Northern Hemisphere (Cheng, 1984). The model assumes permafrost may exist at elevations above the lower limit:

$$H = 3650\times \exp\left(-0.003(\varphi - 25.37)^2\right) + 1428 \quad (1)$$

For the MAGT model, Nan *et al.* (2002) related mean annual ground temperature T_{cp} (°C) to elevation E (m asl) and latitude φ (°) with a regression equation based on deep borehole data from the Qinghai–Tibet Highway (QTH) recorded between Golmud and Lhasa in 1980–2000 (Eqn 2). Permafrost is likely to occur when $T_{cp} < 0.5$°C:

$$T_{cp} = -0.83\varphi - 0.0049E + 50.63341 \quad (2)$$

FROSTNUM is a semi-physical model originally proposed by Nelson and Outcalt (1987). The frost number F, calculated from the ground surface freezing index DDF (°C.day) and ground surface thawing index DDT (°C.day), is used to determine the occurrence of permafrost, when $F > 0.5$. Nan *et al.* (2012) added a parameter E to the model:

$$F = \frac{\sqrt{|DDF|}}{\sqrt{|DDF|} + E\sqrt{DDT}} \quad (3)$$

where

$$E = \sqrt{\frac{\lambda_t \cdot Q_f}{Q_t \cdot \lambda_f}}$$

a dimensionless parameter that enables flexibility for parametric optimisation. λ_f and λ_t are the thermal conductivities of the frozen and unfrozen soil (W/(m.°C)), respectively. Q_f and Q_t are the heat fluxes (J/(m^2.s)) released from or absorbed into soil during freezing or thawing periods, respectively. The revised model becomes the original form when $E = 1$. In this study, we define $E = 0.9$, based on a prior determination (Nan *et al.,* 2012).

The TTOP model is another semi-physical model (Riseborough, 2002):

$$TTOP = \frac{(r_k \times n_t \times l_t) - \left(n_f \times l_f\right)}{P} \quad (4)$$

where $r_k = \lambda_t/\lambda_f$ is the ratio of the soil's thawed and frozen thermal conductivities, respectively; n_t and n_f are the n-factors during thawing and freezing periods, respectively, which have been well studied on the QTP (Li & Wu, 2004); l_t and l_f are the thawing index and freezing index of air temperature (°C.day), respectively; and P is the period, which is considered 365 days for a regular year. Permafrost areas have $TTOP \leq 0$. Equation 4 becomes Eqn 5, which we adopted in this study, if the ground surface thawing index and freezing indices (DDT and DDF) are employed:

$$TTOP = \frac{r_k \times DDT - DDF}{P} \quad (5)$$

The K-MODEL is a relatively complex model proposed by Kudryavtsev *et al.* (1974) to estimate the temperature at the bottom of the active layer (T_z), which is equivalent to the temperature at the top of permafrost in the TTOP model. The original form considers the effects of buffer layers such as vegetation and snow cover. With the direct input of ground surface temperature (GST), the model takes the form:

$$T_z \frac{0.5T_s(\lambda_f + \lambda_t) + A_s \frac{\lambda_f - \lambda_t}{\pi}\left(\frac{T_s}{A_s}\arcsin\frac{T_s}{A_s} + \sqrt{1 - \frac{\pi^2}{A_s^2}}\right)}{\lambda} \quad (6)$$

where T_s and A_s are the GST and its amplitude, respectively. The denominator λ depends on the sign of numerator, which will be λ_f if the numerator is negative and otherwise λ_t. Permafrost is likely to occur when $T_z < 0$.

Study Area and Data

The QTP covers 2.62 × 10^6 km^2, bounded by longitudes 75.69–104.43°E and latitudes 26.00–39.82° N (Figure 1). The elevations gradually decrease from west to east, with an average of 4000–5000 m asl. The Qiangtang High Plain (QHP), located in the northwest QTP, has well-developed permafrost. The eastern QTP comprises rugged mountains, except in the Qaidam basin, where the city of Golmud is situated.

The remote sensing data used were from the Moderate Resolution Imaging Spectroradiometer (MODIS) land surface temperature (LST) product and Shuttle Radar Topography Mission (SRTM) digital elevation model (DEM), which were processed into 1 × 1 km spatial resolution for the period 2003–12. Glacier data were obtained from the *Second Glacier Inventory Dataset of China* (Guo *et al.,* 2015), which represents conditions in 2010. The lake data were a subset from the 1 : 250 000 *Topographic Map of China* (National Geomatics Center of China, 2008). Records of measured daily mean GST for 2003–12 were obtained from 71 weather stations on the QTP (Figure 1). The *Map of Frozen Soil Distribution on Qinghai–Tibet Plateau* (PERM-MAP) (Li & Chen, 1996), which is based on observations along the QTH and expert opinions, was used to evaluate the model results. The coordinate systems were standardised to the Albers equal-area conic projection and the Krasovsky ellipsoid in accordance with China's survey standard.

We collected laboratory-tested thermal conductivity data from QTP soils. The data were few and far from a full representation of soil conditions over the entire region. The thermal conductivity of a particular soil type may exhibit strong spatial heterogeneity but lies within the plausible ranges listed in Table 1, originally presented by Wright *et al.,* (2003). The soil type on the QTP can be identified on the map *Quaternary Geology and Geomorphology in the Qinghai–Tibet Plateau and its Adjacent Areas* (Xiang *et al.,* 2013). Thus, we generated a pair of random values for frozen and unfrozen thermal conductivities for each grid cell, constrained by the corresponding ranges in Table 1.

During 2008–12, a permafrost survey project entitled *Permafrost Background Survey on the Qinghai–Tibet Plateau* was carried out, in which five areas and many line transects were comprehensively investigated. Three areas (Wenquan, Gaize and West Kunlun; Figure 1) were identified as representative of broader landform characteristics, permafrost type and thermal state in the region.

The Wenquan area (2584 km^2), located in the eastern QTP, has high and rugged mountains, with elevations ranging from 3430 to 5300 m asl. Glaciers and lakes cover 113 km^2. Permafrost in the area is of island type. The Gaize area covers 41 251 km^2, including 200 km^2 of lakes. It is generally flat, with an average altitude of 4700 m asl, and

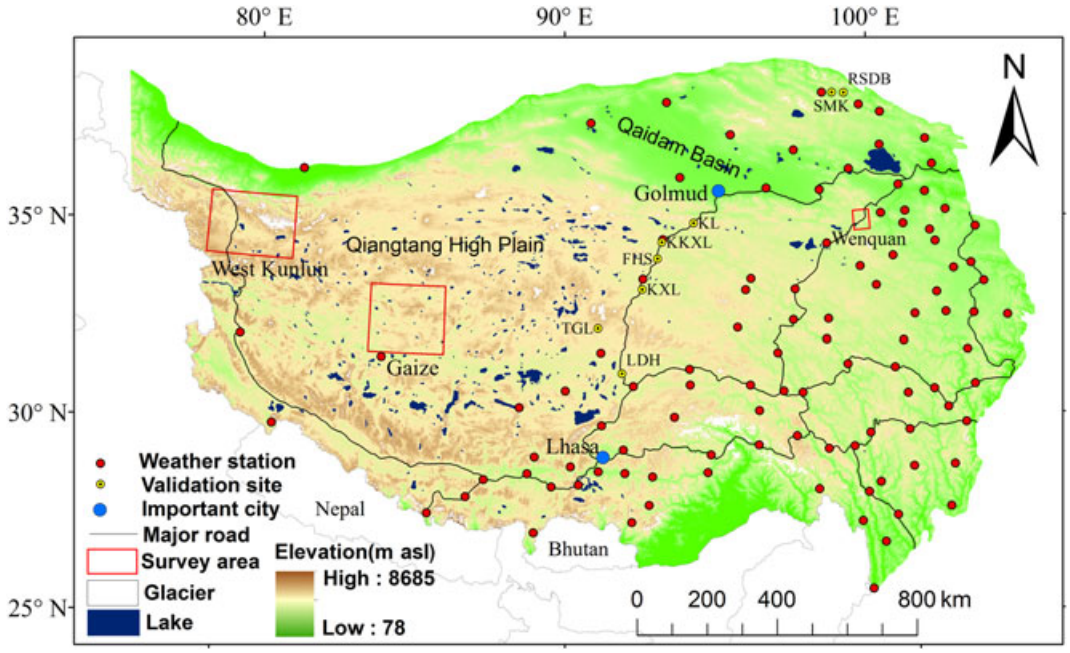

Figure 1 Location map showing the topography and elevation of the QTP and weather stations, validation sites and three typical survey areas (Wenquan, Gaize and West Kunlun). [Colour figure can be viewed at wileyonlinelibrary.com]

Table 1 Typical values of dry density and thermal conductivity of frozen and unfrozen soils developed on different types of surficial deposits (Wright *et al.,* 2003).

Soil type	Dry density (kg/m^3)	λ_t (W/(m·°C))	λ_f (W/(m·°C))
Colluvial	1400	1.15–1.54	1.61–2.69
Lacustrine	1475	1.21–1.62	1.82–2.74
Aeolian	1500	1.39–1.60	1.63–2.47
Glaciofluvial	1550	1.26–1.66	1.65–2.50
Alluvial	1600	1.30–1.72	1.59–2.53
Glacial till	1750	1.41–1.98	1.68–2.92
Organic	300	0.52	1.70

is a transition area between continuous and island permafrost. There are no glaciers in the area. The West Kunlun area in the northwest QTP is at high elevation, ranging from 4400 to 5600 m asl. The area covers about 43 593 km^2, of which glaciers and lakes constitute 6252 km^2. Permafrost is continuous and stable in this alpine environment.

Survey-based permafrost distribution maps (INVEST-MAP) are available for the three areas. The maps represent conditions in 2010, because they are based on abundant and detailed survey data from that year. The INVEST-MAPs were therefore considered as 'true' when evaluating the model outputs. The original spatial resolution of INVEST-MAP is 250 × 250 m, but this was scaled up to 1 × 1 km using the nearest neighbour method.

Estimation of Daily Ground Surface Temperature

The three semi-physical models (FROSTNUM, TTOP and K-MODEL) require GST as the upper boundary condition, which is difficult to obtain from observations because of the limited distribution of weather stations on the QTP. A combined wavelet–ANFIS model was thus adopted to estimate daily GST from four instantaneous observations of MODIS LST spanning 2003–12. Huang and Nan (2013) suggested that a better estimation can be achieved with an optimal wavelet decomposition function and additional time variables. The predictors in this study included the four MODIS LST observations, longitude, latitude, elevation, slope, aspect and sunrise time. The reverse biorthogonal 3.1 wavelet function and three decomposition layers were used.

Ten-year (2003–12) records of observed daily mean GST data from 60 of 71 weather stations were used to train the model. The remaining 11 stations were used for validation. The absolute error and Nash–Sutcliffe correlation coefficient were 1.934 K and 0.982, respectively, in the training stage and 1.956 K and 0.981 in the validation stage. The linear trend lines are close to the 1: 1 line, and the multiple correlation coefficients were both 0.968, suggesting good agreement between the simulated and observed values (Figure 2). The independent variable coefficient was 0.968 for the training stage and 0.984 for the validation stage. To use all available observations, the 71 station records were input to the wavelet–ANFIS model to train a final model, with which the GST over the entire QTP was predicted and used for further model evaluation.

There were numerous missing data from MODIS LST over the QTP due to cloud cover, which resulted in missing GST values. We aggregated 10-year daily GST to obtain multiple-year daily means. The statistics indicated that most of the grid cells had three or more valid daily GST values in the 10 years. The cells that contained no data accounted for about 1.8 per cent of the total; values for these cells were interpolated by ordinary Kriging.

Evaluation Method

The five models were all run at 1 km spatial resolution. The patterns of simulated results were examined by visual inspection and measured with two statistical metrics, namely overall accuracy and Kappa coefficient (Sim & Wright, 2005). Besides the comparisons between models, the results were also compared to PERM-MAP. A higher overall accuracy and greater Kappa coefficient indicate high spatial similarities, with a Kappa coefficient greater than 0.8 suggesting a perfect match (Sim & Wright, 2005).

Outputs (MAGT, TTOP) from the models were compared to values from some observation sites on the QTP. The number of field measurement sites is limited, and they are distributed primarily along the QTH (Figure 1). The field data were therefore of limited utility for verifying the

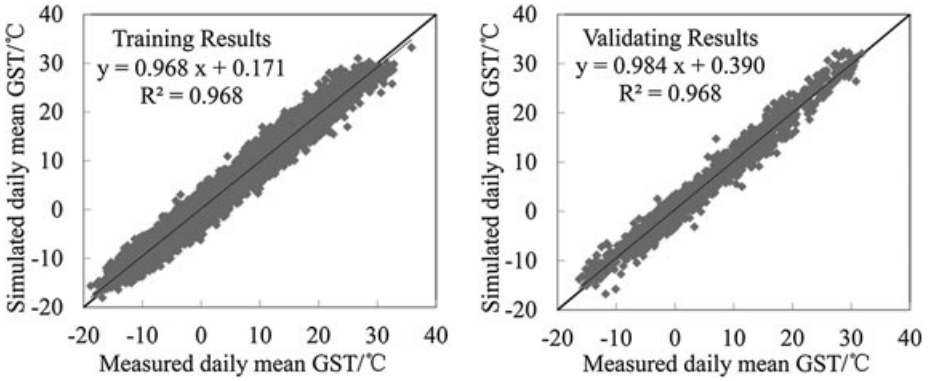

Figure 2 Relationship between simulated and measured daily mean GST in the training and validation stages using the combined wavelet–ANFIS model.

model performance, and so the verification was enhanced by comparing the model results with data from the surveyed areas of Wenquan, Gaize and West Kunlun.

The model performance was also investigated in different elevation ranges and sub-regions with varying field site density. For this assessment, the QTP was classified into three elevation ranges: <3800, 3800–4500 and >4500 m asl (Figure 3). The areas below 3800 m asl include the north, east and southeast edges of the QTP, and the Qaidam basin in the northeast. Areas with elevations between 3800 and 4500 m asl are in the transition areas from the eastern QTP to the interior, and some isolated areas in the central southern part. A vast extent of the central–western QTP has elevations above 4500 m asl. The whole region was roughly divided into three areas based on the availability of data (Figure 3). There are numerous data from area I because many permafrost investigations have been focused along the QTH. Data from these sites form the basis of the PERM-MAP. Areas II and III were delineated based on existing maps. Area II is in continuous permafrost and area III is underlain by island permafrost.

RESULTS

Simulations of the Entire QTP

Figure 4 presents the simulated patterns of permafrost on the QTP from the five selected models, with the PERM-MAP for reference. All the maps show consistent spatial patterns. There is a large extent of permafrost on the QHP in the northern QTP, and island or sporadic permafrost in the eastern QTP, the Qaidam basin and the southern QTP. These broad distribution characteristics are also apparent on the PERM-MAP. The differences between the models are mainly around the edges of the QHP, where permafrost gradually becomes discontinuous and transitions to seasonally frozen ground. The differences are also apparent on the eastern plateau in the mountains.

More permafrost coverage is yielded from the ELEV model on the QHP than from the other models and the PERM-MAP. Elevation is the critical factor controlling permafrost distribution in this area, which is accounted for in ELEV. However, other local factors not accounted for in the model may prevent the formation of permafrost. Thus, ELEV is likely to overestimate permafrost extent in northern Tibet. Nevertheless, ELEV (Figure 4a) and MAGT (Figure 4b) simulated less permafrost coverage than the other three models in the eastern areas with moderately high and rugged mountains (Figure 4c–e).

Table 2 presents the areas of permafrost obtained from the five model simulations and the PERM-MAP, excluding areas covered by glaciers and lakes (97.0×10^3 km^2). The simulated permafrost areas from the TTOP and ELEV models were greatest, with 1.461×10^6 and 1.389×10^6 km^2, respectively. The MAGT permafrost distribution was smallest (1.144×10^6 km^2). The FROSTNUM and K-MODEL were similar in modelled permafrost areas, with 1.219×10^6 and 1.268×10^6 km^2, respectively. The permafrost area on the PERM-MAP is similar to the FROSTNUM and K-MODEL values (1.298×10^6 km^2). The TTOP results indicate much more permafrost along the QTH, and do not match results from field investigations

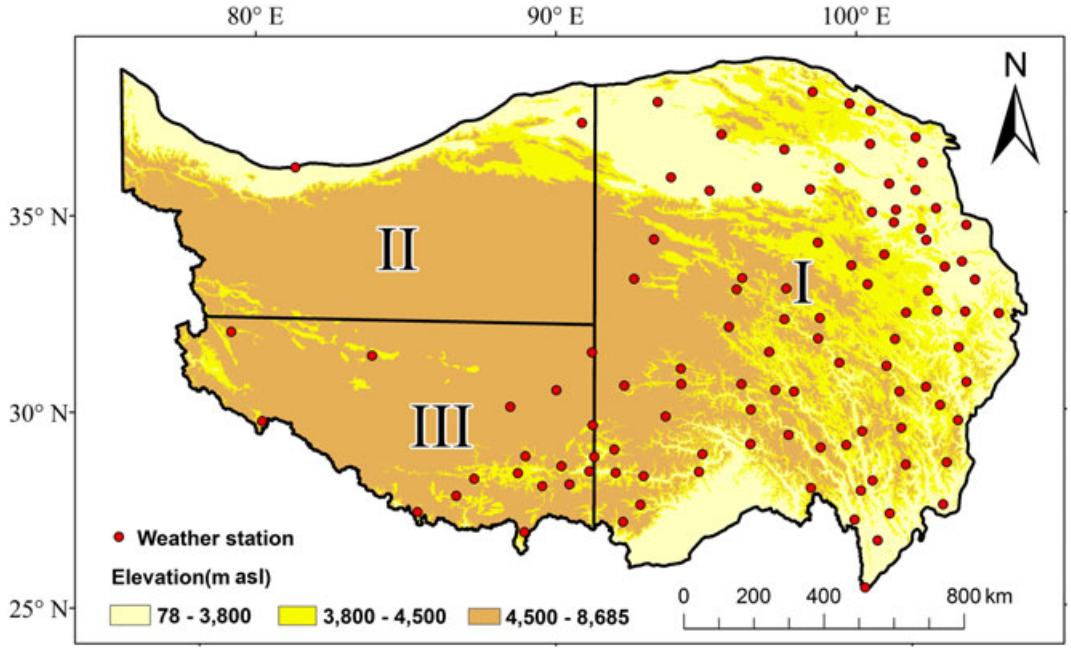

Figure 3 Division of sub-regions based on elevation range and site density. [Colour figure can be viewed at wileyonlinelibrary.com]

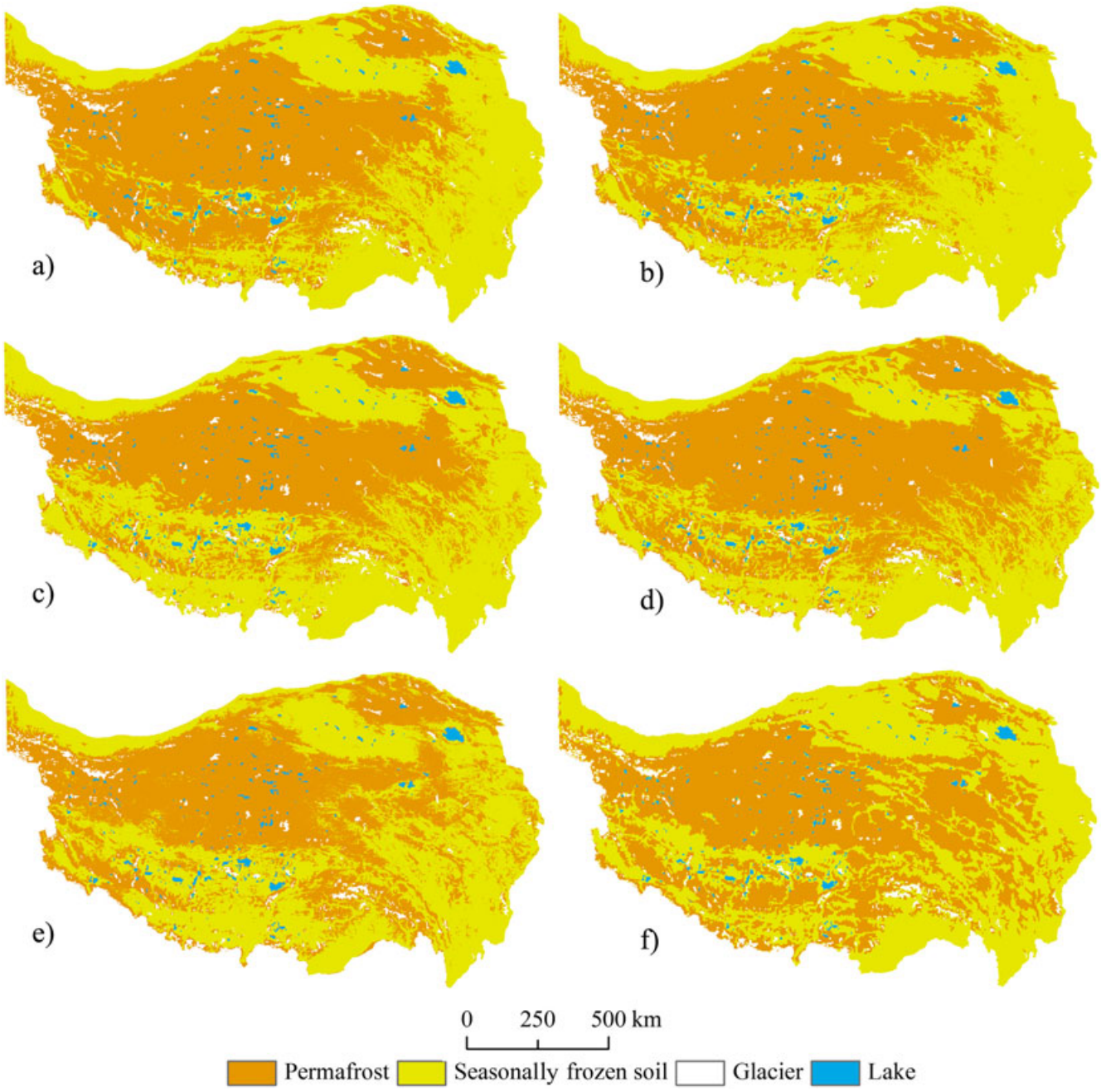

Figure 4 Permafrost distribution maps from the five model simulations: (a) ELEV, (b) MAGT, (c) FROSTNUM, (d) TTOP, (e) K-MODEL and (f) digitised PERM-MAP (published in 1996). [Colour figure can be viewed at wileyonlinelibrary.com]

Table 2 Frozen ground areas simulated by the five models and from the PERM-MAP.

	ELEV	MAGT	FROSTNUM	TTOP	K-MODEL	PERM-MAP
Permafrost ($\times 10^6$ km^2)	1.389	1.144	1.219	1.461	1.268	1.298
Seasonally frozen ground ($\times 10^6$ km^2)	1.133	1.379	1.303	1.061	1.255	1.224

conducted during the engineering of the highway and railway. The limited permafrost coverage from the MAGT model is associated with the regression used in this method, because the annual mean ground temperature in undisturbed parts of the plateau is not represented by borehole records from disturbed sites along the QTH.

Table 3 Spatial similarity between the models and the PERM-MAP over the entire QTP. Values indicate overall accuracy (%) and values within parentheses are Kappa coefficients.

	MAGT	FROSTNUM	TTOP	K-MODEL	PERM-MAP
ELEV	89.9 (0.93)	84.6 (0.90)	85.4 (0.90)	80.9 (0.86)	77.9 (0.85)
MAGT	—	87.3 (0.92)	83.9 (0.89)	83.1 (0.87)	78.0 (0.85)
FROSTNUM	—	—	90.2 (0.94)	84.8 (0.90)	77.7 (0.84)
TTOP	—	—	—	81.7 (0.88)	77.3 (0.85)
K-MODEL	—	—	—	—	74.6 (0.82)

The models and the PERM-MAP were compared by determining the overall accuracy and the Kappa coefficient (Table 3). The overall high similarity metrics indicate good consistency among the models, and between the models and the PERM-MAP. The highest overall accuracy (90.2%) was found between FROSTNUM and TTOP, and the lowest (74.6%) was between the K-MODEL and PERM-MAP. Similarly, the highest Kappa (0.94) was also between FROSTNUM and TTOP and the lowest (0.82) was between the K-MODEL and PERM-MAP. Both FROSTNUM and TTOP use the same surface ground freezing and thawing indices derived from daily GST. These same inputs probably contributed to the high spatial similarity between the two models. However, the differences between them in calculated permafrost area are remarkable (up to 0.242×10^6 km^2), and mainly concentrated in island permafrost areas on the southern QTP.

The similarity between ELEV and the other four models is high, with most Kappa values greater than 0.85. This indicates that elevation is an important factor controlling the distribution of permafrost on the QTP. The similarity between MAGT and the other models is also high, with overall accuracies >83.1 per cent, and Kappa values >0.87. Although the model was based on out-of-date data from 1980 to 2000, the regressed coefficients still perform reasonably. This is probably because mean annual ground temperatures used in the model were measured deep below ground, usually at 10–15 m, and so are more stable than GST variables used in the semi-physical models. The spatial similarity between MAGT and PERM-MAP is high, with a 78 per cent overall accuracy and Kappa value of 0.85. This high similarity is probably because both the MAGT and the PERM-MAP are based on borehole records along the QTH.

In comparison with the similarities between the models and the PERM-MAP (74.6–78.0% overall accuracy, and Kappa values from 0.82 to 0.85), the inter-model similarities are higher, with overall accuracy ranging from 80.9 to 90.2 per cent and Kappa values of 0.86–0.94. The results from the models show consistent similarities, but the differences between the models and the PERM-MAP are distinct. In other words, it is not the model structure that causes differences between any one model and the PERM-MAP, but rather the various time periods that the models and the PERM-MAP represent, the potential errors in the PERM-MAP, and the uncertainties in driving data and parametric settings.

Validation at Typical Sites and Surveyed Areas

The models used in this study have been previously tested for applicability. For example, ELEV was tested in the Qilian mountains (Zhang *et al.,* 2016), MAGT in the Qinghai–Tibet engineering corridor (Lu *et al.,* 2013), FROSTNUM at the Xidatan and Liangdaohe sites in eastern Tibet (Nan *et al.,* 2012), TTOP along the QTH (Wu *et al.,* 2002) and the K-MODEL in the source area of the Yellow River (Luo *et al.,* 2014).

In this study, eight extra representative sites with observations from around 2010 were selected to validate the models. The sites were distributed in a transect along the QTH (Figure 1). Table 4 lists field observations from the sites and the modelled results. Among the sites, Reshui Daban Pass (RSDB) is in seasonally frozen ground (Wang *et al.,* 2013) and the others, namely Shimiankuang Fork (SMK), Kunlun Pass (KL), Kekexili (KKXL), Fenghuoshan

Table 4 Observed variables and simulation results of the five models at some typical sites.

		RSDB	SMK	KL	KKXL	FHS	KXL	TGL	LDH
Observed variables	Longtitude (°E)	38.75	38.78	35.62	35.15	34.73	33.95	32.97	31.82
	Latitude (°N)	99.13	98.75	94.07	93.05	92.90	92.40	91.02	91.73
	Elevation (m)	3609	4132	4746	4734	4896	4652	5100	4808
	MAGT (°C)	2.40	−1.75	−3.00	−2.40	−2.85	−0.77	−1.60	−0.65
	TTOP (°C)	—	−1.55	−2.72	−2.35	−2.82	−0.25	−1.50	−1.00
	Frozen soil type	Seasonally				Permafrost			
Simulation results	H (ELEV) (m)	3561	3556	4091	4168	4234	4355	4497	4650
	T_{cp} (MAGT) (°C)	0.79	−1.80	−2.19	−1.74	−2.18	−0.34	−1.72	0.66
	F (FROSTNUM)	0.54	0.60	0.59	0.57	0.57	0.53	0.58	0.50
	TTOP (TTOP)(°C)	−1.58	−4.20	−3.14	−2.45	−2.59	−1.31	−2.80	−0.45
	T_z (K-MODEL) (°C)	−0.33	−2.56	−3.48	−3.11	−2.92	−1.25	−2.76	−2.16

(FHS), Kaixinling (KXL), Tanggula Pass (TGL) and Liangdaohe (LDH), are underlain by permafrost (Han, 2008; Zhao *et al.,* 2010; Ma *et al.,* 2013). The simulations are in good agreement with the measured field conditions (Table 4). At the seven permafrost sites, elevations are higher than the lower limit of permafrost occurrence calculated by ELEV. ELEV incorrectly modelled permafrost at RSDB, when in fact the site is in seasonally frozen ground. The actual site elevation and calculated lower limit of permafrost are quite close, and so local factors may therefore control the presence or absence of permafrost. Ground temperatures calculated by the MAGT model are comparable with field observations. Annual mean ground temperature in the field was above 0°C at RSDB, confirming that the site is in seasonally frozen ground. The LDH site, however, was incorrectly simulated, probably because permafrost there is close to 0°C and thermally unstable. The FROSTNUM model simulated conditions well for most sites except RSDB and LDH. The temperatures from the TTOP and K-MODEL were generally lower than measured values, suggesting that these models may have overestimated permafrost distribution in the region. These comparisons with field conditions suggest that all models perform poorly at sites with thermally unstable frozen soils, such as RSDB and LDH.

Figure 5 and Table 5 show the model simulations in the three surveyed areas (Wenquan, Gaize, West Kunlun) where the investigation maps for 2010 are available for validation. All models overestimated permafrost distribution in the three areas compared to the INVEST-MAP.

In the mountainous Wenquan area, elevation strongly controls the patterns of permafrost distribution. Consequently, permafrost distribution from the ELEV and MAGT models, which both account for elevation, are more similar spatially to the INVEST-MAP than the other models. Overall accuracies were 84.1 and 90.3 per cent, with Kappa values of 0.58 and 0.77, respectively. The permafrost extent from these models was greater than in the survey, probably because climatic warming in recent decades following the time of model establishment has resulted in permafrost thaw. The simulated permafrost distribution from MAGT was closest to the INVEST-MAP. The three semi-physical models were poorer at capturing permafrost spatial patterns, indicating that they are still too simple to represent terrain-controlled impacts. Among them, the K-MODEL performed slightly better.

The terrain in the Gaize area is moderately flat and underlain by island permafrost near 0°C, which is sensitive to degradation from climate warming. The regional permafrost distribution is mainly controlled by local factors rather than elevation. As a result, neither ELEV nor MAGT reproduced the permafrost distribution well, with low overall accuracies of 50.0 and 54.7 per cent, respectively. The three semi-physical models, which include climatic inputs and soil properties, appear more suitable in this transitional area, with overall accuracies of 73.4, 61.5 and 63.1 per cent (Table 5). However, parameter settings and input data still contribute to the model biases. All the models dramatically overestimated permafrost area in this region.

In the continuous permafrost of the West Kunlun area, all model simulations were in good agreement with the survey, with overall accuracies all above 91 per cent. FROSTNUM had the highest overall accuracy (98.5%) and Kappa coefficient value (0.88). The elevations in the area are high enough to maintain permafrost, and so the ELEV and MAGT models also performed well. The simulated permafrost distribution from K-MODEL was the closest to the INVEST-MAP, but there was more seasonally frozen ground simulated in the southwest part.

Evaluation in Elevation Zones

It is typically assumed that areas at elevations lower than 3800 m asl on the QTP are in seasonally frozen ground. Within this elevation range, the similarities among the models and the PERM-MAP were high, indicating that all the models can simulate the distribution of seasonally frozen ground in this zone (Table 6). The Kappa coefficients are small because the type of seasonally frozen ground accounts for the large majority and Kappa penalises the overall accuracy with its overall probability of random agreement (Brennan & Prediger, 1981).

Areas between 3800 and 4500 m asl are mainly transition zones between seasonally frozen ground in the eastern QTP and continuous permafrost in the plateau interior. Differences between the simulation results and the PERM-MAP are apparent, with overall accuracies <64.4 per cent and Kappa values of 0.19–0.28. Most areas on the QTP are above 4500 m asl (Figure 3). The similarity metrics for this zone are generally lower than for the <3800 m asl zone, and higher than for the 3800–4500 m asl zone. The differences between the models, and between the models and the PERM-MAP, are particularly apparent in the southern area of island permafrost.

The greatest difference between model simulations were in areas at 3800–4500 m asl, and in the southern area of the zone at >4500 m asl. This suggests that the use of uniform parameters for each elevation zone is insufficient. Model performance could be improved by treating elevation zones separately in the simple models. In addition, the high similarities between the models in each elevation zone further confirm that the model structure is not the fundamental source of the discrepancies (Table 6).

Evaluation in Sub-Regions with Different Field Data Availability

The results of similarity assessments in the three sub-regions with various field data availability are listed in Table 7. Although the PERM-MAP is two decades old, it is still used as a reference for permafrost distribution on the QTP. The overall accuracies of the models compared to the PERM-MAP were highest in area II. This area

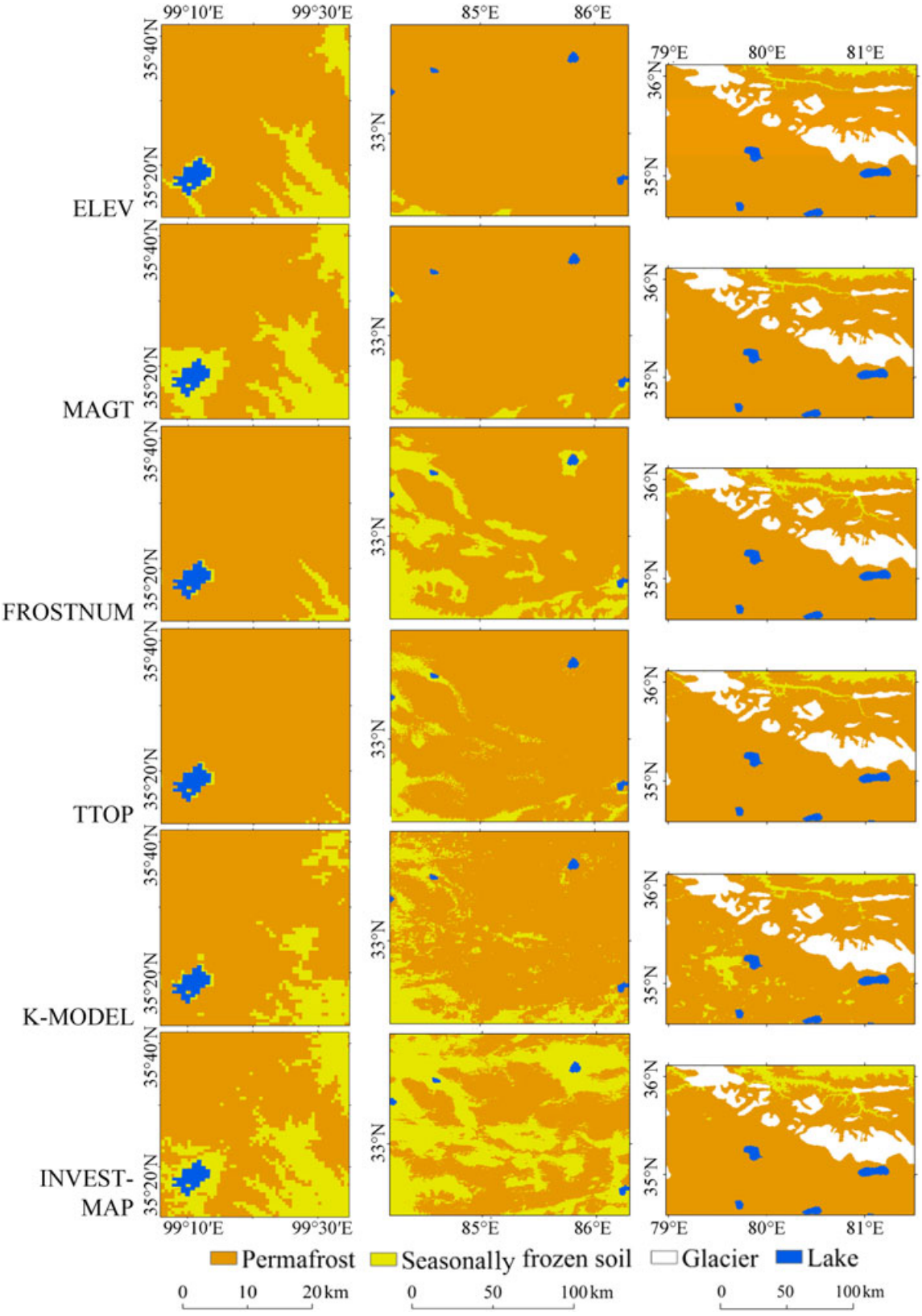

Figure 5 Simulated results in the three surveyed areas: Wenquan (left column), Gaize (middle column) and West Kunlun (right column). [Colour figure can be viewed at wileyonlinelibrary.com]

Table 5 Permafrost area and similarity metrics between the models and the INVEST-MAP in the three surveyed regions.

		INVEST-MAP	ELEV	MAGT	FROSTNUM	TTOP	K-MODEL
Wenquan	Permafrost (km^2)	1678	2056	1752	2400	2461	2124
	Seasonally frozen soil (km^2)	793	415	719	70	11	344
	Overall accuracy (%)	—	84.1	90.3	70.9	68.5	78.7
	Kappa coefficient	—	0.58	0.77	0.13	0.03	0.43
Gaize	Permafrost (km^2)	19 785	40 266	38 318	30 171	35 534	32 632
	Seasonally frozen soil (km^2)	21 266	785	2733	10 880	5516	8421
	Overall accuracy (%)	—	50.0	54.7	73.4	61.5	63.1
	Kappa coefficient	—	0.03	0.12	0.48	0.25	0.27
West Kunlun	Permafrost (km^2)	34 762	36 389	36 219	35 117	36 017	35 054
	Seasonally frozen soil (km^2)	2579	952	1122	2224	1325	2286
	Overall accuracy (%)	—	95.0	95.5	98.5	96.1	91.7
	Kappa coefficient	—	0.49	0.56	0.88	0.65	0.37

Table 6 Spatial similarity metrics within elevation ranges, that is <3800, 3800–4500 and 4500 m asl. Values indicate overall accuracy (%) and values within parentheses are the Kappa coefficients.

	MAGT	FROSTNUM	TTOP	K-MODEL	PERM-MAP
<3800 m					
ELEV	98.1 (0.82)	95.3 (0.68)	87.9 (0.44)	88.9 (0.44)	89.9 (0.16)
MAGT	—	94.6 (0.63)	86.6 (0.39)	88.1 (0.40)	90.7 (0.13)
FROSTNUM	—	—	91.5 (0.61)	89.8 (0.49)	88.9 (0.23)
TTOP	—	—	—	86.4 (0.31)	82.9 (0.21)
K-MODEL	—	—	—	—	83.6 (0.17)
3800–4500 m					
ELEV	91.6 (0.83)	85.0 (0.70)	78.7 (0.58)	80.2 (0.60)	63.1 (0.24)
MAGT	—	80.3 (0.61)	72.6 (0.46)	78.5 (0.57)	62.2 (0.21)
FROSTNUM	—	—	90.0 (0.80)	79.8 (0.59)	64.4 (0.28)
TTOP	—	—	—	75.2 (0.50)	63.3 (0.28)
K-MODEL	—	—	—	—	59.7 (0.19)
>4500 m					
ELEV	85.4 (0.63)	79.7 (0.51)	86.4 (0.63)	77.5 (0.44)	78.2 (0.34)
MAGT	—	86.7 (0.69)	87.0 (0.64)	82.7 (0.57)	78.3 (0.46)
FROSTNUM	—	—	89.9 (0.71)	84.7 (0.62)	78.0 (0.47)
TTOP	—	—	—	82.4 (0.57)	80.0 (0.45)
K-MODEL	—	—	—	—	76.2 (0.42)

Table 7 Spatial similarity between the models and the PERM-MAP in sub-regions with different field data availability (areas I, II and III).

		ELEV	MAGT	FROSTNUM	TTOP	K-MODEL
I	Overall accuracy (%)	75.7	73.7	74.9	72.7	70.1
	Kappa coefficient	0.49	0.43	0.48	0.47	0.39
II	Overall accuracy (%)	90.3	91.1	90.3	90.1	89.1
	Kappa coefficient	0.72	0.75	0.74	0.73	0.70
III	Overall accuracy (%)	68.2	73.2	70.2	73.1	68.6
	Kappa coefficient	0.36	0.46	0.40	0.46	0.38

comprises the QHP, with continuous permafrost. Despite the limited field data available from this sub-region, the high elevations and cold conditions ensure the widespread development of permafrost, leading to consistently high agreement between the models and map sources, with overall accuracies >89 per cent and Kappa values >0.70.

Overall accuracies were about 70 per cent in areas I and III, being slightly higher in area I. Although area I contained

the most data, all model results were found to differ considerably from the PERM-MAP, due to complex topography in the region between 3800 and 4500 m asl, where the models were found to perform poorly (e.g. previous sub-section). The differences between the models and the PERM-MAP were largest in area III, which had the lowest accuracy metrics. Limited field survey data in this area and the unstable ground thermal conditions in transitional areas such as Gaize resulted in poor model performance.

DISCUSSION

The novel contribution of this study was the attempt to make comprehensive comparisons and evaluate model performance through multiple approaches. The spatial similarity metrics indicated that the results from ELEV and MAGT were similar, as were those from FROSTNUM and TTOP, in the three representative areas and for the entire QTP. The performance of the models varies in representative areas, different elevation zones and sub-regions with varying amounts of field data. As a result, the inclusion of regional or altitudinal characteristics may improve model performance. The evaluation also highlighted scale effects of the models. The ELEV and MAGT models included effects of primary controlling factors such as elevation and latitude, but did not account for local factors that may strongly influence the distribution of permafrost in smaller areas. In contrast, the FROSTNUM, TTOP and K-MODEL performed better in areas with island permafrost and particularly in flat terrain, due to the inclusion of external driving forces and soil properties.

The empirical models (ELEV and MAGT) have time-specific parameters. The ELEV regression was based on data from 1955 to 1984, while MAGT used observations from 1980 to 2000. Therefore, the coefficients in the model equations represent conditions in the past rather than at present. Recent climate warming on the QTP has caused permafrost degradation in some areas with warm permafrost (Nan *et al.,* 2003; Cheng & Wu, 2007) and an increase in the lower elevational limit of permafrost (Wu *et al.,* 2005). Not accounting for recent warming probably contributed to inaccuracies in the results from the two empirical models. The effects could have been considerable in the warm and thermally unstable permafrost areas such as Gaize. The same issue exists for the PERM-MAP, which was produced in 1996. As a result, we cannot determine the ability of any one model based solely on the agreement with the PERM-MAP. Instead, their applicability may be inferred by combining inter-model comparisons, site and areal validation, and field expertise.

Both ELEV and MAGT included broad-scale controlling variables such as latitude and elevation. They did not incorporate external freezing and thawing processes or soil properties. Consequently, they did not include the effects of local factors such as slope, aspect, vegetation and snow cover. This leads to significant overestimation of permafrost distribution in the Gaize area, where local factors control permafrost formation. Although the original model coefficients were used in this study, the results suggest that the coefficients could be optimised to better represent current conditions.

The three semi-physical models (FROSTNUM, TTOP and K-MODEL) do not have time-specific parameters, so they can theoretically model any period. However, two factors introduce uncertainty into the mapping. These include the soil thermal conductivities, and the GSTs that were derived from the MODIS LST data through a wavelet–ANFIS approach. Soil properties were simplified in this study to assume single soil columns with uniform frozen and unfrozen thermal conductivity values, due to the lack of available field data. This approach does not capture the effect of soil heterogeneity. Furthermore, organic matter was not included in the model, which may be important to the thermal properties of plateau soils. In the permafrost transition area of Gaize, soil properties play an important role in the development and persistence of permafrost. The difference in frozen and unfrozen soil thermal conductivity can introduce strong thermal offsets that can preserve permafrost even under conditions with mean annual surface temperatures above 0°C. Insufficient consideration of soil heterogeneity and the thermal offset in the simple models allows for the development and application of physically explicit land surface models.

The quality of the estimated GST is critical for an accurate simulation using the semi-physical models. GST is closely related to air temperature but also modified by spatially heterogeneous surface conditions such as snow cover, vegetation and surface soil properties. In some studies, the seasonal *n*-factor approach is used to estimate GST from air temperature (Lunardini, 1981). This method is simple to employ, but *n*-factors may vary considerably, both seasonally and annually, making reliable implementation difficult (Li & Wu, 2005). The present study attempted to extract GST from a remote sensing product using a mathematical approach, to avoid the extensive use of buffer layer data. The MODIS LST data of the study area have been validated for applicability to some degree in previous studies in the Qilian Mountains and at the Litang site in the eastern QTP (Yu *et al.,* 2014; Min *et al.,* 2015). The average absolute deviation of MODIS LST is about 2 K. The biases in the conversion to GST are acceptable ($<$2 K), which is indicated by the multiple-folded cross-validation method.

However, the simplified nature of the GST conversion approach inevitably introduces uncertainty to the results. Vegetation cover on the QTP is sparse, and so its effects can be negligible in some areas. Thick snow cover in the cold season may heavily impact estimations of ground temperature in most permafrost regions (Zhang, 2005). However, the impact of thin snow cover, as characterises the QTP, may be relatively small in comparison (e.g. Wang *et al.,* 2012; Jin *et al.,* 2008). Jin *et al.* (2008) found that the effect of snow cover on GST is weak when snow depth is $<$200 mm. A maximum mean snow depth on the QTP of 142 mm has been inferred using passive microwave

remote-sensing data (Che *et al*., 2008). However, most areas are covered by snow <50 mm deep. To better assess the possible impacts of snow cover, we used a sub-time series from October to April in the cold season to train a new model for determining GST from the MODIST LST data. This approach did not noticeably improve model performance in the cold seasons. The effects of buffer layers such as vegetation and snow cover are implicitly accounted for in the training process of the neural network in the wavelet–ANFIS approach, even though there are no explicit inputs of buffer layers.

The areas occupied by glaciers and lakes were simply excluded from modelled areas. This exclusion may not be ideal because some glaciers and lakes may be underlain by permafrost. However, considering the small overall extent of glaciers and lakes on the QTP (97×10^3 km^2), this would have a small effect on the results compared to other sources of uncertainly in the models.

CONCLUSIONS

The results and discussion of this multi-model comparison of permafrost distribution on the QTP allow the following conclusions to be drawn.

The five empirical and semi-physical models examined in this study captured the broad characteristics of permafrost distribution on the entire QTP, where continuous permafrost is found on the northern QHP, and island permafrost underlies the southern and eastern plateau and the northern Qaidam basin. All models simulated permafrost distribution in areas with colder, continuous permafrost, but performance varied in the mountainous eastern regions and the southern transition regions between island and continuous permafrost.

Both empirical and semi-physical models overestimated the permafrost distribution in three areas surveyed in the field for validation. The empirical models (ELEV and MAGT) performed poorly for thermally unstable areas such as Gaize, where permafrost distribution is mainly affected by local factors not accounted for in the models. Three semi-physical models (FROSTNUM, TTOP and K-MODEL) were better at simulating areas with island permafrost, and particularly in areas with flat terrain, due to the incorporation of GST and soil properties. The results from the elevation model (ELEV) and mean annual ground temperature model (MAGT) were consistently similar in field surveyed areas and over the entire QTP, as were results from the FROSTNUM and TTOP models.

Model performance varied in different elevation ranges and sub-areas. Large variations were found at elevations from 3800 to 4500 m asl and in the southern sub-region dominated by island permafrost. Model performance could probably be improved by explicitly considering the effects of elevation zones and regional characteristics, and with improved availability of data on boundary conditions and soil properties.

Finally, results from all the models were similar over the entire QTP, indicating that model structure is not the fundamental source of the modelling discrepancies. Modelling accuracy is affected by the use of outdated field data in the models' calibration, and simplifications of the surface and subsurface conditions. We recommend that a new permafrost map should be produced for the QTP based on all currently available data. This could serve as an updated reference map for future model evaluation.

ACKNOWLEDGEMENTS

This study was financially supported by the grants from the National Natural Science Foundation of China (No. 41471059), National Science Research Program (No. 2013CBA01803), Open Fund of State Key Laboratory of Frozen Soil Engineering of China (No. SKLFSE201504) and Priority Academic Program Development of Jiangsu Higher Education Institutes (No. 164320H116). We thank Dr. Brendan O′Neil from the University Centre in Svalbard for greatly improving the English text and also extend special thanks to all our colleagues who participated in the project of *Permafrost Background Survey on the Qinghai–Tibet Plateau* and often worked for over 3 months every year on the extremely high QTP.

REFERENCES

Brennan RL, Prediger DJ. 1981. Coefficient Kappa: some uses, misuses, and alternatives. *Educational and Psychological Measurement* **41**: 687–699. DOI:10.1177/001316448104100307

CAREERI/CAS. 2005. Map of Glacier, Permafrost and Desert in China (1 : 4,000,000). SinoMaps Press: Beijing, China [in Chinese].

Che T, Li X, Jin R, Armstrong R, Zhang TJ. 2008. Snow depth derived from passive microwave remote-sensing data in China. *Annals of Glaciology* **49**: 145–154. DOI: 10.3189/172756408787814690

Chen H, Nan ZT, Zhao L, Ding YJ, Chen J, Pang QQ. 2015. Noah modelling of the permafrost distribution and characteristics in the west Kunlun area, Qinghai–Tibet Plateau, China. *Permafrost and Periglacial Processes* **26**: 160–174. DOI:10.1002/ppp.1841

Cheng GD. 1984. Problems on zonation of high-altitude permafrost. *Acta Geographica Sinica* **39**: 185–193. [in Chinese with English abstract]

Cheng GD, Wu TH. 2007. Responses of permafrost to climate change and their environmental significance, Qinghai-Tibet Plateau. *Journal of Geophysical Research: Earth Surface* **112**: DOI:10.1029/2006JF000631F02S03

Cheng WM, Zhao SM, Zhou CH, Chen X. 2012. Simulation of the decadal permafrost distribution on the Qinghai–Tibet Plateau (China) over the past 50 years. *Permafrost and Periglacial Processes* **23**: 292–300. DOI:10.1002/ppp.1758

Guo WQ, Liu SY, Xu JL, Wu LZ, Shangguan DH, Yao XJ, Wei JF, Bao WJ, Yu PC, Liu Q, Jiang Z. 2015. The second Chinese glacier inventory: data, methods and results. *Journal of Glaciology* **61**: 357–372. DOI: 10.3189/2015JoG14J209

Han LM. 2008. Study on stability for low embankment of Qinghai-Tibet railway in Tanggula Mountain permafrost area. Doctoral Dissertation, Beijing Jiaotong University [in Chinese with English abstract].

Huang PP, Nan ZT. 2013. Estimation of 0-cm soil temperature over the Tibetan Plateau based on the Wavelet analysis and adaptive network-fuzzy inference system. *Journal of Glaciology and Geocryology* **35**: 74–83. [in Chinese with English abstract]

Jin HJ, Sun LP, Wang SL, He RX, Lv LZ, Yu SP. 2008. Dual influences of local environmental variables on ground temperatures on the interior-eastern Qinghai–Tibet Plateau (I): vegetation and snow cover. *Journal of Glaciology and Geocryology* **30**: 535–545. [in Chinese with English abstract]

Juliussen H, Humlum O. 2007. Towards a TTOP ground temperature model for mountainous terrain in central-eastern Norway. *Permafrost and Periglacial Processes* **18**: 161–184. DOI:10.1002/ppp.586

Kudryavtsev VA, Graragula LS, Kondratev VG. 1974. Foundation of Geocryology. Moscow State University Press: Moscow, Russia.

Li J, Sheng Y, Wu JC, Chen J, Zhang XM. 2009. Probability distribution of permafrost along a transportation corridor in the northeastern Qinghai Province of China. *Cold Regions Science and Technology* **59**: 12–18. DOI:10.1016/j.coldregions.2009.05.012

Li SD, Chen GD. 1996. Map of Frozen Soil Distribution on Qinghai–Tibet Plateau (1 : 3,000,000). Gansu Cultural Press: Lanzhou, China [in Chinese].

Li SX, Wu TH. 2004. Permafrost temperature regime: study method and applied analysis. *Journal of Glaciology and Geocryology* **26**: 377–383. [in Chinese with English abstract]

Li SX, Wu TH. 2005. The relationship between air temperature and ground temperature in the Tibetan Plateau. *Journal of Glaciology and Geocryology* **27**: 627–632. [in Chinese with English abstract]

Li X, Cheng GD. 1999. A GIS-aided response model of high-altitude permafrost to global change. *Science in China Series D: Earth Sciences* **42**: 72–79. DOI:10.1007/BF02878500

Lu JH, Niu FJ, Cheng H, Lin ZJ, Liu H, Luo J. 2013. The permafrost distribution model and its change trend of Qinghai-Tibet engineering corridor. *Journal of Mountain Science* **31**: 226–233. [in Chinese with English abstract]

Lunardini VJ. 1981. Heat Transfer in Cold Climates. Van Nostrand Reinhold: New York, USA.

Luo DL, Jin HJ, Marchenko S, Romanovsky V. 2014. Distribution and changes of active layer thickness (ALT) and soil temperature (TTOP) in the source area of the Yellow River using the GIPL model. *Science China Earth Sciences* **57**: 1834–1845. DOI:10.1007/s11430-014-4852-1

Ma W, Mu YH, Li GY, Wu QB, Liu YZ, Sun ZZ. 2013. Response of embankment thermal regime to engineering activities and climate change along the Qinghai–Tibet railway. *Scientia Sinica Terrae* **43**: 478–489. [in Chinese]

Min WB, Li YQ, Zhou J. 2015. Validation of MODIS land surface temperature products in east of the Qinghai-Xizang Plateau. *Plateau Meteorology* **34**: 1511–1516. [in Chinese with English abstract]

Nan ZT, Gao ZS, Li SX, Wu TH. 2003. Permafrost changes in the northern limit of permafrost on the Qinghai–Tibet Plateau in the last 30 years. *Acta Geographica Sinica* **58**: 817–823. [in Chinese with English abstract]

Nan ZT, Huang PP, Zhao L. 2013. Permafrost distribution modeling and depth estimation in the Western Qinghai-Tibet Plateau. *Acta Geographica Sinica* **68**: 318–327. [in Chinese with English abstract]

Nan ZT, Li SX, Cheng GD, Huang PP. 2012. Surface Frost Number Model and its application to the Tibetan Plateau. *Journal of Glaciology and Geocryology* **34**: 89–95. [in Chinese with English abstract]

Nan ZT, Li SX, Liu YZ. 2002. Mean annual ground temperature distribution on the Tibetan Plateau: permafrost distribution mapping and further application. *Journal of Glaciology and Geocryology* **24**: 142–148. [in Chinese with English abstract]

National Geomatics Center of China. 2008. Topographic Map of China (1 : 250 000). Sinomap Press: Beijing, China.

Nelson FE, Outcalt SI. 1987. A computational method for prediction and regionalization of permafrost. *Arctic and Alpine Research* **19**: 279–288. DOI:10.2307/1551363

Ran YH, Li X, Cheng GD, Zhang TJ, Wu QB, Jin HJ, Jin R. 2012. Distribution of permafrost in China: an overview of existing permafrost maps. *Permafrost and Periglacial Processes* **23**: 322–333. DOI:10.1002/ppp.1756

Riseborough D, Shiklomanov N, Etzelmüller B, Gruber S, Marchenko S. 2008. Recent advances in permafrost modelling. *Permafrost and Periglacial Processes* **19**: 137–156. DOI:10.1002/ppp.615

Riseborough DW. 2002. The mean annual temperature at the top of permafrost, the TTOP model, and the effect of unfrozen water. *Permafrost and Periglacial Processes* **13**: 137–143. DOI:10.1002/ppp.418

Sim J, Wright CC. 2005. The kappa statistic in reliability studies: use, interpretation, and sample size requirements. *Physical Therapy* **85**: 257–268.

van der Velde R, Su Z, Ek M, Rodell M, Ma Y. 2009. Influence of thermodynamic soil and vegetation parameterizations on the simulation of soil temperature states and surface fluxes by the Noah LSM over a Tibetan plateau site. *Hydrology and Earth System Sciences* **13**: 759–777. DOI:10.5194/hess-13-759-2009

Wang K. 2009. A Study on Simulation of the Permafrost Distribution in Qinghai-Tibet Plateau Based on RS/GIS. Doctoral Dissertation, Jilin University, Changchun, Jilin, China [in Chinese with English abstract].

Wang QF, Zhang TJ, Wu JC, Peng XQ, Zhong XY, Mu CC, Wang K, Wu QB, Cheng GD. 2013. Investigation on permafrost distribution over the upper reaches of the Heihe river in the Qilian mountains. *Journal of Glaciology and Geocryology* **35**: 19–29. [in Chinese with English abstract]

Wang XQ, Lu XY, Wang JF. 2012. The relationship between air temperature and ground, snow or grass temperature under the conditions of different snow depth. *Desert & Oasis Meteorology* **41**: 1068–1072. [in Chinese with English abstract]

Wright JF, Duchesne C, Côté MM. 2003. Regional-scale permafrost mapping using the TTOP ground temperature model. In Proceedings of Eighth International Conference on Permafrost, Marcia P, Springman SM, Arenson LU (eds). AA Balkema Publishers: Zurich, Switzerland; 1241–1246. Vol. 2

Wu QB, Zhu YL, Liu YZ. 2002. Application of the permafrost table temperature and thermal offset forecast model in the Tibetan Plateau. *Journal of Glaciology and Geocryology* **24**: 614–617. [in Chinese with English abstract]

Wu TH, Li SX, Cheng GD, Nan ZT. 2005. Using ground-penetrating radar to detect permafrost degradation in the northern limit of permafrost on the Tibetan Plateau. *Cold Regions Science and Technology* **41**: 211–219. DOI:10.1016/j.coldregions.2004.10.006

Xiang SY, Wang A, Wang GC, Zeng FM, Lu JF, Jiang SS, Chang H, Lin X, Lu YL. 2013. Quaternary Geology and Geomorphology of the Qinghai-Tibet Plateau and Its Adjacent Areas (1 : 3000 000). China University of Geosciences Press: Wu Han, China [in Chinese].

Xiao Y, Zhao L, Dai YJ, Li R, Pang QQ, Yao JM. 2013. Representing permafrost properties in CoLM for the Qinghai-Xizang

(Tibetan) Plateau. *Cold Regions Science and Technology* **87**: 68–77. DOI:10.1016/j.coldregions.2012.12.004

Yang K, Chen Y-Y, Qin J. 2009. Some practical notes on the land surface modeling in the Tibetan Plateau. *Hydrology and Earth System Sciences* **13**: 687–701. DOI:10.5194/hess-13-687-2009

Yu WP, Ma MG, Wang XF, Geng LY, Tan JL, Shi JN. 2014. Evaluation of MODIS LST products using longwave radiation ground measurements in the northern arid region of China. *Remote Sensing* **6**: 11494–11517. DOI:10.3390/rs61111494

Zhang TJ. 2005. Influence of the seasonal snow cover on the ground thermal regime: an overview. *Reviews of Geophysics* **43**: 1159–1162. DOI:10.1029/2004RG000157

Zhang WJ, Ren ZP, Yao L, Zhou CH, Zhu YQ. 2016. Numerical modeling and prediction of future response of permafrost to different climate change scenarios on the Qinghai–Tibet Plateau. *International Journal of Digital Earth* **9**: 442–456. DOI:10.1080/17538947.2015.1041431

Zhang XM, Nan ZT, Wu JC, Du EJ, Wang T, You YH. 2013. Mountain permafrost distribution modeling using multivariate adaptive regression spline (MARS) in the Wenquan area over the Qinghai–Tibet Plateau. *Science in Cold and Arid Regions* **4**: 361–370.

Zhao L, Wu QB, Marchenko SS, Sharkhuu N. 2010. Thermal state of permafrost and active layer in Central Asia during the international polar year. *Permafrost and Periglacial Processes* **21**: 198–207. DOI:10.1002/ppp.688